Chapter 5

Simultaneous Measurement of fMRI and EEG – Principles and Applications

Yeji Han, Sung Suk Oh, Joong Koo Kang and HyunWook Park

Additional information is available at the end of the chapter

http://dx.doi.org/10.5772/31194

1. Introduction

Functional MRI (fMRI) and electroencephalogram (EEG) are the most widely used neuroimaging techniques which assist neuroscientists in investigating human brain function. FMRI measures the induced magnetic field change, usually the change in the blood oxygenation level dependent (BOLD) contrast, which reflects physiological changes of neuronal activity (Ogawa et al., 2000). EEG measures the summed electrical activities of neurons by detecting the electric potential difference at the scalp. As the sources of the signal measured by fMRI and EEG are different, the spatial and temporal information of the two techniques are also different. For example, EEG has millisecond resolution which is much higher than fMRI's temporal resolution, characterized by the lag of the hemodynamic response of 6-7 seconds (Friston et al., 1998). Low temporal resolution of fMRI is inevitable not only because the BOLD contrast is developed over seconds by accumulated changes of the magnetic field, resulting from neuronal activities and vascular changes (Rosenkranz & Lemieux, 2010), but also because several seconds are required to perform each MRI measurement. Instead, fMRI has excellent spatial resolution which is much higher than EEG. Moreover, the spatial as well as the temporal resolution of fMRI is expected to further increase as the field strength of MRI system is still increasing (Ogawa et al., 2000; Regatte et al., 2007). Thus, EEG and fMRI are complementary for brain research in regard to the types of information they can provide, and it is important to utilize both EEG and fMRI signals to get a more comprehensive view of brain activities.

To combine the information provided by fMRI and EEG, one can consider performing data fusion after separately acquiring data using each modality, as it is done for many other multimodality approaches such as combining MRI with positron emission tomography (PET) or combining MRI with computed tomography (CT). Combining PET or CT images with MR

images is rather straight-forward because only a correct image registration process is required for a successful fusion of multimodality data. Combining EEG and fMRI data is more complicated; the two types of data are different as fMRI data is presented in the image domain whereas EEG represents information using waveforms in the time domain. Thus, it is recommended to simultaneously acquire fMRI and EEG data so that the data can be more easily interpreted afterwards. In fact, when fMRI and EEG are simultaneously measured, a more accurate interpretation of the data is possible because the timing information is commonly available for both of the measurements, making it more concise to figure out which parts of the fMRI and EEG signals originated from the identical brain activity.

While simultaneous recording of the two modalities can provide high spatio-temporal information for brain research, there are several issues that have to be considered to successfully perform a simultaneous fMRI-EEG measurement, such as patient safety, fMRI image quality, and EEG quality. Patient safety and image quality can be usually coped by using a properly designed MR-compatible EEG instrument. However, degradation of EEG quality cannot be prevented during the acquisition process and several post-processing techniques have to be employed to remove artefacts in the acquired EEG data.

In this chapter, a practical approach for simultaneous fMRI and EEG measurement will be discussed in detail. In section 2, an actual measurement technique and required hardware/software will be presented. Then, common artefacts of EEG signal and removal techniques will be discussed in section 3. In section 4, a practical example of simultaneous fMRI-EEG experiment will be demonstrated.

2. Simultaneous measurement of EEG and fMRI

The first report on a combined use of fMRI and EEG was presented in 1993 (Ives et al., 1993), which showed that signals of brain activities could be obtained with both high spatial and high temporal resolution. In the following years, more experiments have been conducted to confirm the possibility of recording EEG inside an MR scanner (Huang-Hellinger et al., 1995; Lemieux et al., 1997). Nowadays, it has become more common to measure fMRI and EEG simultaneously and many practical applications have been introduced for epilepsy, sleep, and other brain functions.

When an experiment with a simultaneous measurement of fMRI and EEG is conducted, the first step is to prepare a proper EEG instrument. The EEG instrument is composed of electrodes which detect the EEG signal and a recording system which amplifies and digitizes the detected EEG signal. To record EEG signal within an MRI system, electrodes are attached to the patient head and placed inside an MR scanner while the recording system (the amplifier and the digitizer) is placed inside or outside the MR scanner according to different needs. Thus, it should be guaranteed that the electrodes are made with MRcompatible materials because anything placed inside an MR scanner should not contain ferrous material due to safety as well as potential susceptibility artifacts in the MR image. If an experiment requires the amplifier and digitizer placed inside the MR scanner, it should be ensured that they are

http://dx.doi.org/10.5772/31194

manufactured with MR-compatible materials and can operate properly in the high magnetic field.

For EEG quality, the number of electrodes located at the subject's brain scalp is a critical factor because it determines the overall spatial resolution (Reilly, 2005) and the numbers of electrodes in commercially available EEG instrument ranges from 32 to 256. Another factor which influences the EEG quality is the arrangement of electrodes and electrode wires connected to the amplifier/digitizer. To prevent possible signal artefact induced by the magnetic field change, they have to be set on the subject's head without any loops. To minimize the problems related to the electrodes and the electrode wires, an electrode cap is generally used (Bonmassar et al., 2002; Srivastava et al., 2005). In addition, immobilization of the subject's head and fixation of the electrode wires are also important factors for the EEG quality, as well as for the fMRI quality, because the change of the loop area created by the electrode wires in the static field also induces artefacts. To reduce movements of the electrodes and the electrode wires, various techniques are being employed, such as weighing down the electrode wires using sandbags (Benar et al., 2003), padding (Hoffmann et al., 2000), and placing a tight bandage over the subject's head (Benar et al., 2003). Additionally, a vacuum cushion is widely used to reduce the subject's head motion (Benar et al, 2003).

For a simultaneous fMRI-EEG experiment, most of the published literature have conducted experiments using either BrainAmp (BrainProducts GmbH, Munich, Germany) or EMR32 (Schwarzer GmbH, Munich, Germany) because both of them allow the use of an amplifier, which is non-magnetic, shielded, battery-operated, and designed for use in the MRI scanning environment. The EEG signals are amplified, converted to digital signals, and transmitted from the MR scanning environment to a computer located in the control room via optical fibers. Figure 1 shows a typical example of the commercially available MRcompatible EEG instruments, which include electrode caps (32 and 64 channels), a vacuum cushion, and a sandbag.

Using a properly prepared EEG instrument, EEG, electrocardiogram (ECG), and electrooculogram (EOG) signals are recorded, usually with a sampling rate of 5 KHz to capture the rapid change of artefacts caused by switching the magnetic field gradients during fMRI acquisition (Allen et al., 2000). After the EEG signal is measured, artefacts have to be removed as explained in the following sections. Attenuation of the artefacts caused by the gradient fields is employed by initially filtering with a cut-off frequency, typically smaller than 70Hz. The resulting signals are then down-sampled to 200 Hz. Since 200Hz is the sampling rate used for the conventional EEG measurement, down-sampling can reduce the processing time without degrading the EEG quality (Allen et al., 2000).

When EEG and ECG signals are measured, the EEG signals can be represented with different montages by using different references (Fisch, 1999). One of the most widely used montages is the referential montage, which defines a reference electrode at an inactive position, such as the midline position between two hemispheres of the brain. The reference may also be defined at such positions, where the distances from the left channel and the corresponding right channel are equal, eg. earlobes. Thus, the referential montage represents the EEG signal compared to the background EEG signal. The bipolar montage refers to the potential difference between two adjacent electrodes, with longitudinally or transversely directed chains (Fisch,

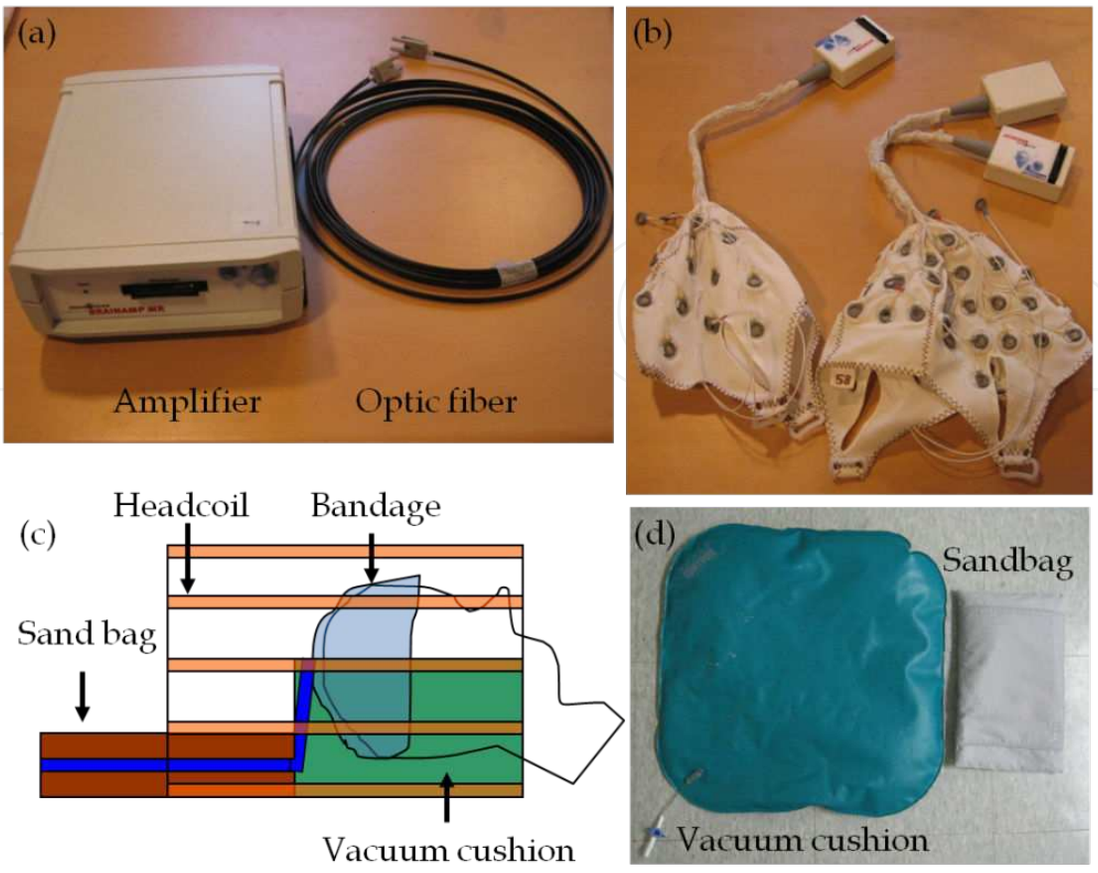

Figure 1. The EEG Instrument. (a) amplifier and optic fiber, (b) electrode caps, (c) illustration of EEG measurement inside an MRI system with an RF headcoil, and (d) aiding materials for movement reduction.

1999). This montage is known to be useful for localization. The third type of montage is the average reference montage, where the common reference is obtained by averaging all EEG signals. Lastly, the Laplacian montage averages several neighboring electrodes surrounding the measured EEG channel and uses the average signal as a reference (Fisch, 1999). For analysis of the EEG signal, any preferred montage can be constructed from the recorded signals in an effort to to clearly demonstrate waveform of EEG events as explained above.

For fMRI measurement, a conventional echo planar imaging (EPI) with the BOLD contrast is generally applied. However, some imaging parameters, such as repetition time (TR), should be carefully chosen to minimize the interference with EEG measurement (Mandelkow et al., 2006). In some cases where fMRI and EEG acquisition has to be recorded for an extended period of time, such as for sleep or epilepsy studies, the data size is too large that the data acquisition has to be performed in several separate sessions.

As briefly mentioned earlier, both the fMRI and the EEG signal can be contaminated when measured simultaneously. Thus, artefacts in the acquired data have to be eliminated before they can be analyzed. The types of artefacts encountered and the artefact reduction techniques that can be applied will be discussed in the following sections.

http://dx.doi.org/10.5772/31194

3. EEG artefacts and their reduction algorithms

When EEG and fMRI are simultaneously measured, both fMRI and EEG signals are influenced by each other. For example, MR image quality may be degraded because the main static field (B0) and the transverse rotational magnetic field (B1) can be altered due to EEG equipment inside the MR room (Mullinger et al., 2008). However, the quality of the MR image is not adversely degraded if the EEG equipment is properly designed and manufactured so that the field inhomogeneities caused by the EEG instrument are minimized. What should be more carefully investigated is the effect of fMRI measurement on the EEG signals, as the EEG quality can be significantly degraded with simultaneous fMRI acquisition, which can induce several types of artefacts, such as (i) image acquisition artefact (IAA); (ii) ballistocardiogram (BCG) artefact; and (iii) quantization error of the analogue-to-digital converter (ADC) (Garreffa et al., 2004). Therefore, when EEG is measured in combination with fMRI, a number of artefact reduction processes have to be employed before it can be used for clinical or research applications.

The two main EEG artefacts are IAA and BCG artefact. The IAA, caused by applied imaging gradient fields during fMRI measurements, is usually removed using periodicity and consistency of the applied gradient fields (Garreffa et al., 2004). The exact cause of the BCG artefacts is not figured out but it is generally known to be added to the EEG signal due to subtle movements of the subject's scalp or abrupt changes of the blood flow in the aortic arch during heartbeats (Ives et al., 1993). The IAA is easier to be removed than the BCG artefact because the former is relatively constant over time when the same imaging gradient is applied for every scan. However, it is rather difficult to remove the BCG artefact because the frequency, shape, and amplitude of the artefact vary from case to case. The third type of artefact is the quantization error. As the amplitude of the IAA can be more than two orders of magnitude higher than that of the EEG signal, the physiological signal in the EEG measurement may be lost if EEG is not measured with sufficient range (Allen et al., 2000).

In the following sections, a detailed explanation of the two main artefacts will be presented and the solutions for these two major artefacts will be discussed.

3.1. Image acquisition artefact (IAA)

The IAA is caused by the changes in the magnetic field during the scanning process, resulting from various factors such as the RF pulses, B^0 field inhomogeneities, body motion, and gradient switching. The switching gradient field, which is inevitable as manipulation of the applied gradient fields plays the main role in acquiring MR images, induces strong artefacts in EEG with an extremely large amplitude. Since the amplitude of IAA is 10~100 times larger than the amplitude of EEG signal, the actual EEG signal is almost completely obscured (Vanderperren et al., 2010). For that reason, earlier studies have performed aperiodic fMRI, where image acquisition is triggered after an EEG event of interest (Krakow et al., 2001). However, EEG-triggered fMRI or interleaved EEG-fMRI measurement is not an optimal solution because it reduces the flexibility of experimental design (Allen et al., 2000).

To remove the IAA from the EEG signal, researchers have focused on the properties of applied gradient fields. Since an MR imaging sequence, mostly the EPI sequence, is repeated during an fMRI experiment, identical changes take place in the gradient fields, inducing the IAA with a consistent shape for each EPI scan. Thus, most algorithms try to eliminate the IAA using the reproducibility and consistency of the IAA shape (Allen et al., 2000).

One of the first IAA reduction algorithms calculated the average IAA spectrum and subtracted the average IAA spectrum from the EEG spectrum (Sijbers et al., 1999; Hoffman et al., 2000). This artefact removal technique is integrated in FEMR software (Schwarzer GmbH, Munich, Germany), which eliminates unwanted signals that are outside the frequency range of the EEG (0.1-40Hz) using band-pass filtering. The artefacts within this frequency range have to be selectively removed. Hoffman's algorithm initially selects 10 different 10s-long sections of EEG acquired inside the magnet, which are unaffected by any artefacts, and uses them as baseline. Then, the frequency spectrum of the baseline is subtracted from the IAA-related spectrum embedded in the EEG signal (Hoffmann et al., 2000). Since IAA is periodic and its frequency range is limited, the removal can be performed in the frequency domain. However, there can be spectral overlap of the IAA and EEG signals in some cases, resulting in an excessive subtraction of the artefact spectrum from the EEG signal.

The other type of IAA reduction algorithm is based on Allen's algorithm (Allen et al., 2000), which is integrated in BrainVision Analyzer (Brain Products GmbH, Munich, Germany). Allen's IAA reduction algorithm consists of two stages: (i) the artefact waveform is averaged over a fixed number of gradient artefact epochs and subtracted from each epoch in the EEG signal; and (ii) the residual IAA is attenuated by a noise cancelling algorithm (Allen et al., 2000). Since template-based removal algorithms typically leave considerable residual noise, further reduction steps should be followed.

More recently, Allen's algorithm has been integrated in parts of many other IAA removal algorithms, including Niazy's algorithm (Niazy et al, 2005), which combines Allen's method with principal component analysis (PCA), and Mantini's algorithm (Mantini et al., 2007), which combines Allen's algorithm with independent component analysis (ICA). A new method to develop a more precise template using a time-continuous cubic spline model has been also presented (Koskinen et al. 2009). Figure 2 shows a typical example of EEG signal recorded inside a 3T MRI scanner (ISOL Technology, Korea). Fig.2 shows the EEG signal with IAA (top) and the signal after the IAA reduction using the BrainVision Analyzer (bottom).

In addition to the above-mentioned algorithms, triggering can be used in combination for detecting the starting point of every scan, which is then used as a marker for more precise averaging of the artefact waveform. Another approach is to perform an interleaved MRI acquisition, where MR acquisition is suspended at regular intervals, resulting in periods free of IAA on the EEG (Ritter et al, 2010).

In general, currently available hardware and software approaches to remove IAA from EEG signal provide satisfactory EEG signals. Moreover, it is less complicated than the removal of the cardiac pulse related artefacts which we discuss below because the timing and shape information of the IAA can be inferred from the applied gradients of MRI.

http://dx.doi.org/10.5772/31194

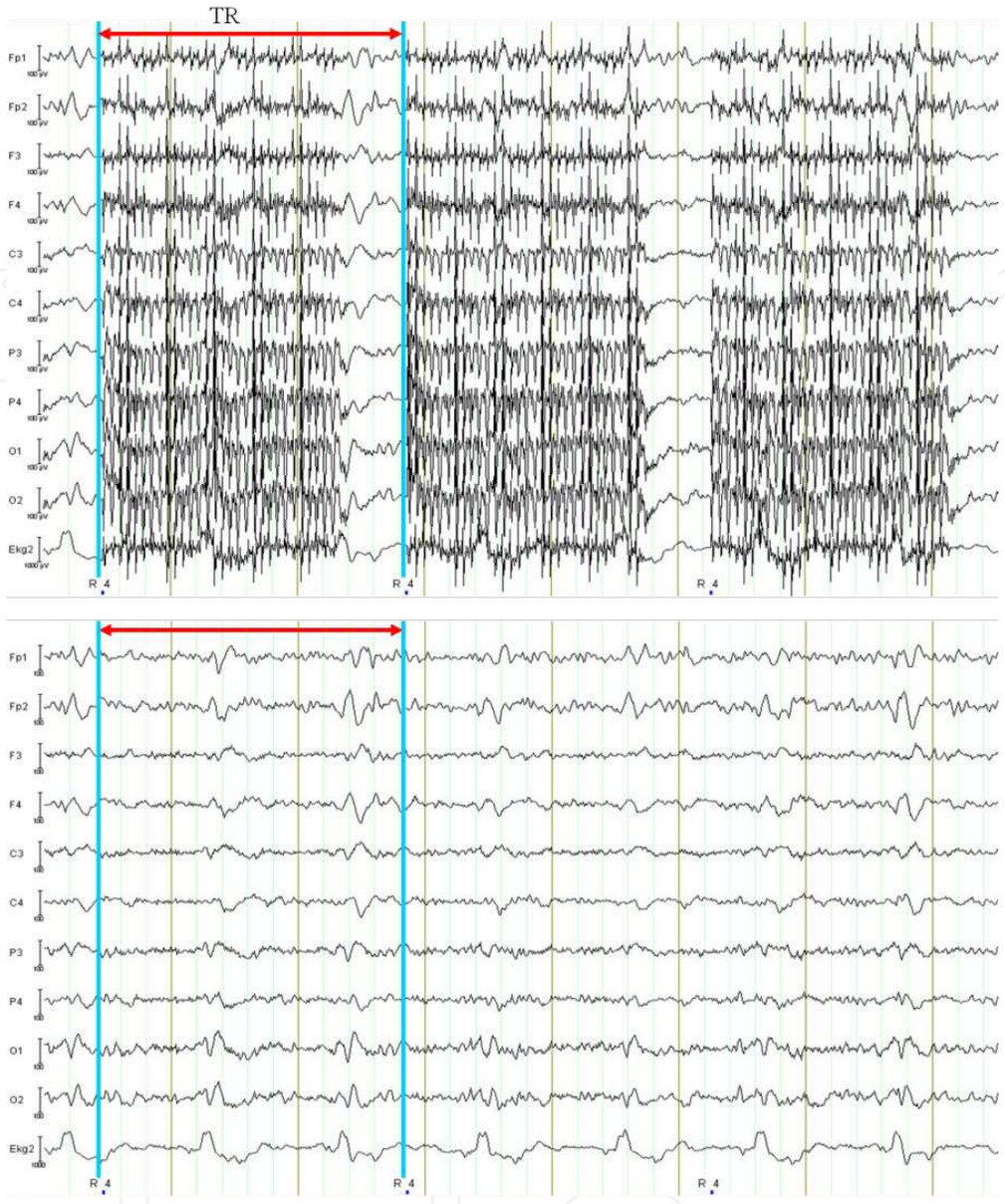

Figure 2. EEG signals recorded from 10 different channels (Fp1, Fp2, F3, F4, C3, C4, P3, P4, O1, O2) and ECG signal with the image acquisition artefact (top) and after the IAA reduction (bottom)

3.2. Cardiac-related artefact

Another EEG artefact that makes the interpretation of the EEG signal rather intricate is the ballistocardiogram artefact (BCG artefact), which is caused by alteration in physiological status. Although the exact cause of the BCG artefact is still being investigated, it is known to be induced by the movement of the patient's body as a result of acoustic vibrations due to the scanner as well as voluntary subject movements (Reilly, 2005). In this chapter, however, we refer to the small involuntary cardiac-related body movements (ballistocardiogram). The BCG artefact can be observed from the EEG signals measured outside an MR scanner but it is small and can be easily removed (Debener et al., 2008). However, the BCG artefact becomes much

greater inside the scanner because of the interaction between the active cardiovascular system and the main static field (B0) (Allen et al., 1998). Consequently, it is observed in the EEG signals measured inside an MR scanner, even when EPI sequences are not applied.

A BCG artefact follows the shape of a cardiac cycle (Fig.3). In fact, the BCG artefact closely follows the cardiac cycle with a delay of approximately 210ms between the R peak of the ECG and the BCG artefact (Allen et al., 1998). Fig.3 also shows that the amplitude of the BCG artefact is comparable, if not slightly larger, to the EEG signal. However, it was predicted that the amplitude of the BCG artefact is proportional to the B0 field (Tenforde et al., 1983), and has been confirmed later (Debener et al., 2008). Debener et al. (2008) showed that the amplitude of the BCG artefact is a function of the static magnetic field strengthand the spatial variability of the BCG artefact substantially increased at higher magnetic field strengths. In reference to various BCG artefacts, Debener et al. has also demonstrated that individual subjects have different heart rates, peak latencies, and shapes (Debener et al., 2008). Moreover, the shapes of the BCG artefact of different EEG channels also vary. As a result, it is difficult to distinguish an 'event' from the EEG signal when the signal is distorted by the BCG artefact.

If the frequency of the BCG artefact is constrained in a certain range distinct from that of the EEG signal, one can think of filtering the artefact in the frequency domain. Although the frequency range of the BCG artefact is mainly in the theta (4-8 Hz) band, however, it can extend to the alpha (8-13 Hz) and delta (0.5-4 Hz) bands, thus overlapping with the EEG signals (Garreffa et al., 2004).

Figure 3. Shows ECG and EEG signals measured inside an MRI scanner without applying the imaging gradients. The BCG artefacts are embedded in each channel.

http://dx.doi.org/10.5772/31194

3.2.1. Average artefact subtraction (AAS)

There are also algorithms that remove the BCG artefacts from the EEG signal based on properties other than the frequency characteristic. One approach to remove the BCG artefact is based on the average artefact subtraction (AAS) algorithm (Allen et al., 1998), which creates an average BCG artefact template/waveform and subtracts it from the EEG signal. It is based on the observation that the shape and the occurrence rate of the BCG artefact is quite consistent across a number of successive heartbeats in each channel of the EEG. Thus, the AAS algorithm consists of two steps: generating an averaged BCG artefact template and subtracting it from the BCG artefact occurrences. First, reference points for each BCG artefact have to be defined. The average waveform is calculated for each referential EEG signal on a second-by-second basis and requires the previous 10 seconds of EEG and ECG signals. The R peak in the QRS complex of the ECG is detected for every heartbeat by thresholding the amplitude of the measured ECG signal using a predefined value and the onset of each BCG artefact is identified using a predefined delay (Allen et al., 1998). Once the onset of every cardiac cycle is detected, a BCG artefact template is generated by averaging the EEG signal over a predefined window size for each EEG channel as the BCG artefact exhibits different shapes in different EEG channels. Finally, the average BCG artefact template is subtracted from the measured EEG signal.

One of the most important steps for the AAS-based algorithms is to find the correct onset points of the BCG artefact because variations of the subject's heartbeat may alter the time delay between the R peak of the QRS complex in the ECG signal and the BCG artefact in the EEG signal. If the onset points are not correct, it is difficult to find the precise average artefact template and the exact reference point for subtraction and this leaves too much residual artefact after subtraction from the EEG signal. Although the AAS method assumes that the shape and occurrence of the BCG artefacts have little variance over time and the condition of the subject's heartbeat is stable, these assumptions may not be necessarily true. Thus, the AAS algorithm has a limitation that the corrected EEG signal can still have residual artefacts due to an inaccurate BCG artefact template.

To account for the shape variations of the BCG artefacts, more algorithms have been introduced to generate BCG artefact templates using other approaches, such as Gaussian weighted averaging (Goldman et al., 2000), median filtering (Sijbers et al., 2000; Ellingson et al., 2004), and wavelet-based adaptive filtering (Kim et al., 2004).

For the AAS-based methods, defining the template length is also an important issue. Since the actual R-R interval is not consistent, the BCG artefact can be subtracted twice if the R-R interval is shorter than the template length and insufficiently subtracted in the other case. To reduce the dependency of the AAS based algorithms on the template length, alternative algorithms have been introduced. One of these scales the template length to a certain percentage of the mean R-R period (Ellington et al. 2004). A plug-in for EEGLAB in FMRIB (http://www.fmrib.ox.ac.uk/eeglab/fmribplugin/), incorporates the BCG artefact data for all R-R period lengths in the current moving average window and the template is adaptively applied to each QRS period based on its R-R period (Brain Vision Analyzer software, http://www.brainproducts.com/). Other algorithms account for the template duration problem using the Kalman

filter (Bonmassar et al., 2002), the EOG signals (In et al., 2006), the recursive least squares motion recording (Masterton et al., 2007), and a moving general linear model (mGLM) (Vincent et al., 2007).

More recently, the optimal basis set (OBS) (Niazy et al., 2005) method was proposed to use a few principal components as representations of several distinct pulse artifact templates. Since these templates include most of the BCG artefact in any given EEG channel and can be used to regress the BCG artefact, the OBS method can account for a greater temporal variation in the BCG artefact shape (Debener et al., 2010). For the OBS method, however, the number of principal components that create the template have to be selected by the user, and thus, affect the performance of this method.

The major advantage of the AAS based algorithms, in comparison with the blind source separation (BSS) algorithm, is low complexity. However, obtaining satisfactory results can be quite difficult because finding the precise onset points of the cardiac cycle for an accurate template is rather complicated as demonstrated by the variants of the AAS method mentioned above.

3.2.2. Blind source separation (BSS)

The AAS based and the OBS based algorithms focus on the fact that the BCG artefact of each EEG-channel has different shapes. However, the BCG artefact can be also characterized by a number of typical topographies (Bénar et al., 2003). Thus, another algorithm to remove the BCG artefacts is based on the blind source separation (BSS) algorithm, which assumes that the characteristics of the BCG artefacts are independent from or orthogonal to the EEG signals (Bénar et al., 2003). The principal or independent components are obtained using the orthogonal or independent characteristics, respectively, between the BCG artefact and EEG activity of the brain. There are several ways to perform the separation of the BCG artefacts and the EEG signal. Early approaches of BSS algorithms are based on manual selection of the independent components, including the original algorithm using ICA (Bénar et al., 2003). In Bénar's algorithm, the components contributing to the BCG artefact are manually identified and taken out from the components. Then, reconstruction of the EEG signal with the remaining free of artefact components can produce EEG signal with reduced artefacts.

More ICA algorithms have been introduced, including Informax ICA, which uses the minimization of the mutual information (Bell & Sejnowski, 1995), FastICA, which uses the maximization of the non-Gaussianity (Hyvärinen & Oja, 2000), joint approximate diagonalization of eigenmatrices (JADE) (Cardoso & Souloumiac, 1993), and second order blind identification (Belouchrani et al., 1993). ICA methods are implemented in the EEGLAB software (http://sccn.ucsd.edu/eeglab/). Since the ICA algorithms reduce the BCG artefact by removing the subjectively defined components that are correlated to the BCG artefact after the ICA processing, the performance may depend on users.

To solve this problem, algorithms for automatic identification of components related to the BCG artefact have been also proposed. Some of the selection criteria for the automatic identification include correlation with the ECG signal (Srivastava et al., 2005; Mantini et al.,

2007), frequency content related to the heartbeat rate and its harmonics (Vanderperren et al., 2007), and autocorrelation of the EEG signal (Deburchgrave et al., 2008; Vandersperren et al., 2010). The BCG-related components can be distinguished by the peaks in their autocorrelation. Because the BCG artefacts are originated from the cardiac pulsing, selection of frequency related components can be based on the harmonics of the heart rates. This property can be exploited as a tool to select the artifact-related components from the ICA decomposition, where the heart rate frequency is determined by computing the inverse of the average distance between consecutive QRS peaks. However, these algorithms require a delicate selection of parameters to achieve better performance (Vanderperren et al., 2010). Moreover, ICA method is inefficient to account for the spatial variation of the BCG artefact since independent components are obtained from EEG signals measured at different positions of the brain. As an alternative, OBS-ICA method can be used, which initially removes a major part of the BCG artifact using the OBS method and then removes the residual BCG artefact using the ICA method. (Debener et al., 2007)

The main advantage of the BSS algorithms is that, unlike the AAS based algorithms, the exact onset of the BCG artefact is not required to be identified. However, the BSS algorithms have higher computational complexity than the AAS algorithms. In addition, the BSS algorithms may not work properly for the EEG signals measured in higher field MRI scanners, i.e., 3T and 7T, as deviations in the spatial information of the BCG artefact become greater in higher field MRI systems (Debener et al., 2008).

3.2.3. Modified average artefact subtraction (MAAS)

As discussed in the previous sections, both ASS and BSS algorithms have advantages and disadvantages. However, for 3T or higher field MRI systems, the ASS algorithms can be more efficient (Vanderperren et al., 2010). To optimize the ASS algorithm for higher field MRI systems, a modified AAS (MAAS) algorithm has been proposed to improve the construction and the subtraction of the BCG template using a fully automatic process (Oh et al., 2014). The MAAS algorithm is composed of two steps; it initially finds an accurate reference point based on the ECG signal to use for the BCG artefact subtraction and the template generation. Then, an accurate BCG artefact subtraction algorithm is applied, which adaptively subtracts the BCG artefact template using different delay and window sizes.

To find the reference points for the BCG artefacts, R peaks of the ECG signal have to be accurately identified. According to Debener (Debener et al., 2007), a negative swing occurs between the S and T states of the P_QRS_T wave due to an axial blood flow momentum when the ECG signal is recorded in a high field MR system. This negative swing is used to automatically identify the R peak from ECG in the MAAS algorithm (Oh et al., 2014). Since an R peak and the following negative peak produce the maximum signal difference, the difference of positive and negative peaks is calculated to deduce the R peak. For each segment of the ECG signal with a predefined duration, a sliding window of 0.3s duration is defined to reflect the physiological characteristic (Debener et al., 2007). Within the sliding window, a positive peak and the following negative peak are identified and the difference between the peaks is calculated. After eliminating the positive and negative peak pairs whose difference is smaller

than the average, the maximum peak among the remaining positive peaks is selected as the R peak candidate of the current window. Then, the false R peaks are eliminated from the candidate peaks using the resting heartbeat rate (Sharieff, 2006). Since the distances between adjacent R peaks should be within 0.5-1.3 seconds (for 46-120 bpm), the R peak candidate is eliminated if its distance from the previous R peak or the following R peak does not lie in this range. After elimination, the point which has the maximum ECG signal is assigned as a new R peak in sections where the distance of adjacent R peaks is larger than 1.3 seconds.

To detect the BCG artefact from the contaminated EEG signal, a BCG clip is defined for the EEG signal using the R peak as shown in Fig.4. After extracting the BCG clips from the current EEG segment, the BCG clips suitable for a correlation template (CT) generation are classified; if the absolute mean of a BCG clip is larger than the absolute mean of BCG from all previous EEG segments, it is not used for CT generation. Then, the remaining BCG clips are averaged to generate the CT, and then correlation coefficients between each BCG clip and the CT are calculated to figure out the true peak of the current BCG artefact. By considering the delay time between an R peak and the following BCG artefact, the BCG artefact is classified into a normal and a deformed BCG artefact.

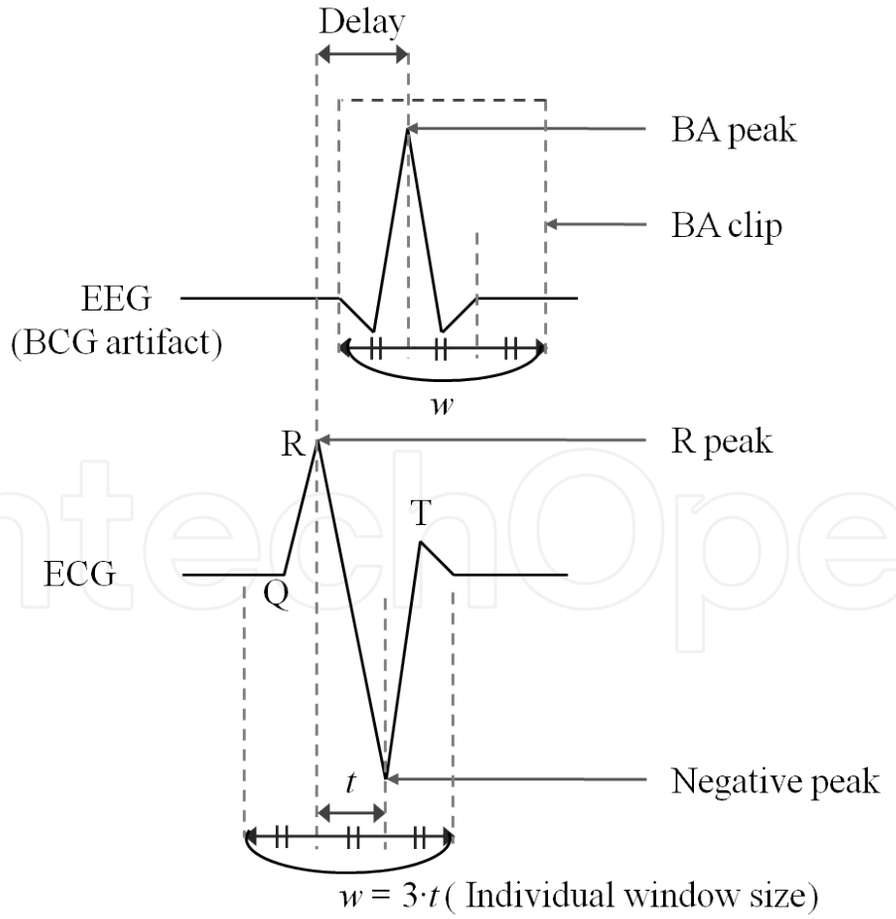

Figure 4. An illustration of the ballistocardiogram (BCG) artifact.

http://dx.doi.org/10.5772/31194

The BCG artefact template is simply obtained by averaging more than two normal BCG artefacts within the current segment, and its length is defined by the maximum window size of the normal BCG artefacts. For a normal BCG artefact, the contaminated EEG signal is corrected by subtracting the BCG artefact template using the individual delay and the individual window size. In case of a deformed BA artefact, the BCG artefact template is subtracted using the average window size and the average delay.

Figure 5 shows the contaminated EEG signal with the BCG artefact and the EEG signal after applying BCG reduction using the OBS, ICA, and MAAS algorithms. Since the MAAS algorithm detects R peaks accurately and uses variable window and delay properties, it can neatly remove the BCG artefacts. Since the OBS method uses the mean R-R interval as the window size of the BCG artefact template, it can result in distortion if the current R-R interval is shorter than the mean R-R interval. In this study, some of the epilepsy signals are overly removed since the mean R-R interval is used. The error is also partly due to the fact that the selected components of the OBS are related to epilepsy signals. For ICA, the estimated BCG artefact cannot handle the variation of the BCG artefacts for every EEG channel and the correction results can have residual artefacts.

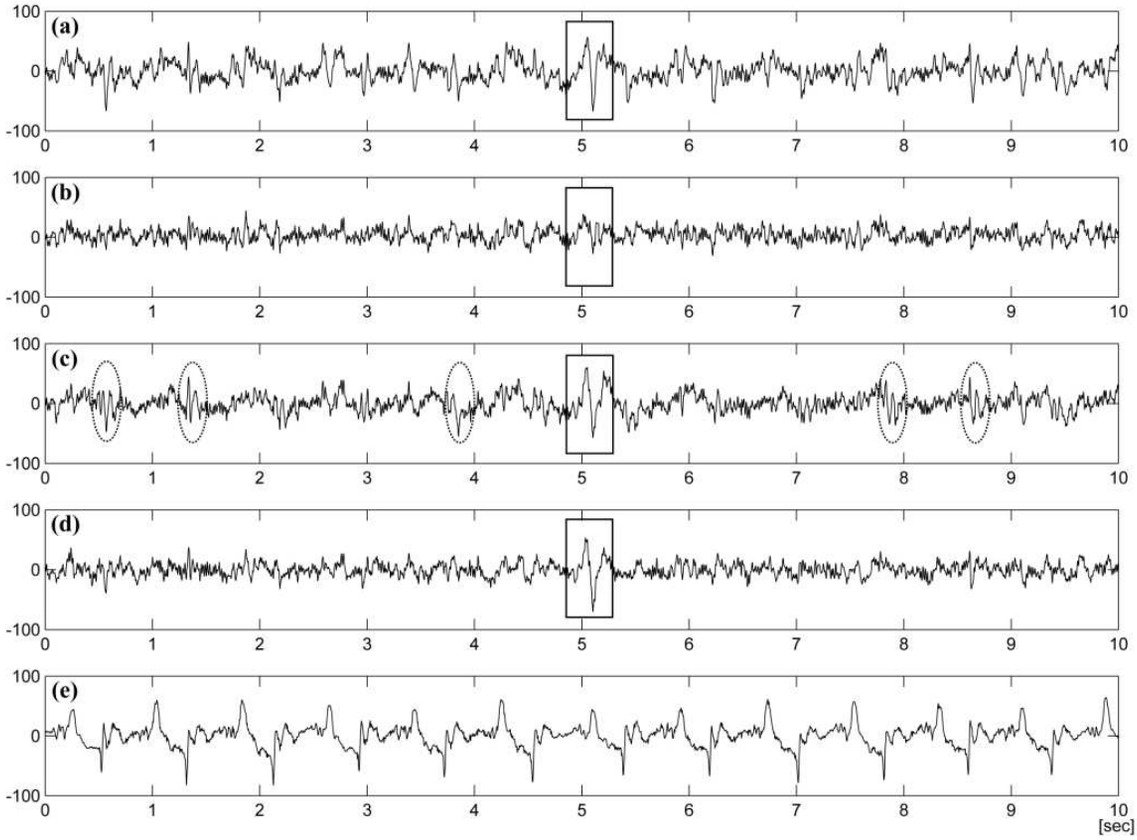

Figure 5. The BCG artefact and its corrected signals. (a) EEG signal on the F7 channel before correction, (b) corrected EEG signal by OBS, (c) corrected EEG signal by ICA, (d) corrected EEG signal by MAAS, and (e) scaled ECG signal. In this study, some of the epilepsy signals are overly removed when the OBS algorithm is used (marked with squares) and the ICA algorithm leaves too much residual BCG artefacts (marked with dotted ovals).

4. Application of fMRI+EEG measurements

The possibility of recording the EEG inside an MR scanner has opened a wide variety of new research areas. Generally, there are three application areas for simultaneous fMRI and EEG studies: neurovascular coupling, cognitive and systems neuroscience, and clinical studies. However, the most straightforward application would be to search for brain activation and deactivation areas related to specific events of the EEG signal. This type of research has been carried on via correlation between the BOLD time series and a postulated EEG-derived model of haemodynamic changes, generated by the general linear models (GLM). In other words, the temporal information acquired from the EEG signals can be used as timing information for the stimulus cue in fMRI. Then, the fMRI analysis can be performed using the MR images corresponding to the cue timing as images of stimulus conditions and the rest as images of reference conditions.

Typical application areas of simultaneous fMRI-EEG experiments include resting state studies such as sleep studies, brain rhythm studies, and activation studies for pain research, auditory research, visual research, and cognition research (Horovits et al., 2008; Christmann et al., 2007; Laufs et al., 2003). In this section, a practical example of a simultaneous fMRIEEG experiment for epilepsy patient is demonstrated. Moreover, three different BCG artefact reduction algorithms are compared using fMRI analysis results.

The development of simultaneous EEG and fMRI measurement was initially motivated out of interest in identifying the BOLD changes related to interictal epileptiform discharges (IED) (Rosenkranz et al., 2010). Although the timing and the shape of epilepsy waveform can be acquired using EEG, spatial information of EEG is not as accurate because the EEG signal is measured at certain locations on the surface of a brain only. Thus, fMRI analysis is used to provide more accurate spatial information of an epilepsy patient by providing not only the cortical but also the subcortical information.

In this experiment, three patients with intractable partial epilepsy were recruited and a written consent was signed by every patient prior to the experiments. A neurologist supervised the experiments to ensure the safety of the patients. EEG recording was performed inside a 3T MRI system (ISOL Technology, South Korea) using BrainAmp and BrainCap (BrainProducts GmbH, Germany). With BrainCap, 21 EEG channels (Fp1, Fp2, F3, F4, C3, C4, P3, P4, O1, O2, F7, F8, T7, T8, P7, P8, Fz, Cz, Pz, TP9, and TP10 in the 10-20 channel system), two ECG channels, and an EOG were recorded during 5 to 7 sessions, each lasting for 11 minutes. The international 10-20 system is an electrode placement scheme mostly applied for epilepsy studies, which is based on the relationship between the location of an electrode and the underlying area of the cerebral cortex. The 10 and 20 represent the distances between adjacent electrodes which are 10% and 20% of the total front-back and right-left distance of the skull (Fisch, 1999). The reference electrode of the cap was located at the mid-points (Cz and Fz), and EEG/ECG signals were recorded with a sampling rate of 5kHz to prevent aliasing.

At the same time, fMRI data was simultaneously acquired using the following imaging parameters: gradient-echo echo-planar-imaging (GE-EPI) sequence, TR/TE=3000/37 msec,

http://dx.doi.org/10.5772/31194

matrix size=64×64, FOV=220×220 mm^2, slice thickness=4 or 5mm, number of slices=20 or 30, and flip angle=70°.

After the measurement, the EEG signals were filtered by a phase-shift-free Butterworth filter having a band-pass range of 0.5 to 55 Hz. IAA was then eliminated using the BrainVision Analyzer (BrainProducts) and the filtered signals were down-sampled to 500 Hz (Mandelkow et al., 2006). To remove the BCG artefacts, ICA, OBS and MAAS algorithms were separately applied to the EEG signals. For fMRI analysis, Statistical Parameter Mapping (SPM8, http://www.fil.ion.ucl.ac.uk/spm/) was used with the pre-processing steps of 'realign' and 'smoothing with a Gaussian filter having a full width at half maximum of 8mm'. For the t-test, p-value of 0.001 and a cluster analysis of 4mm was applied.

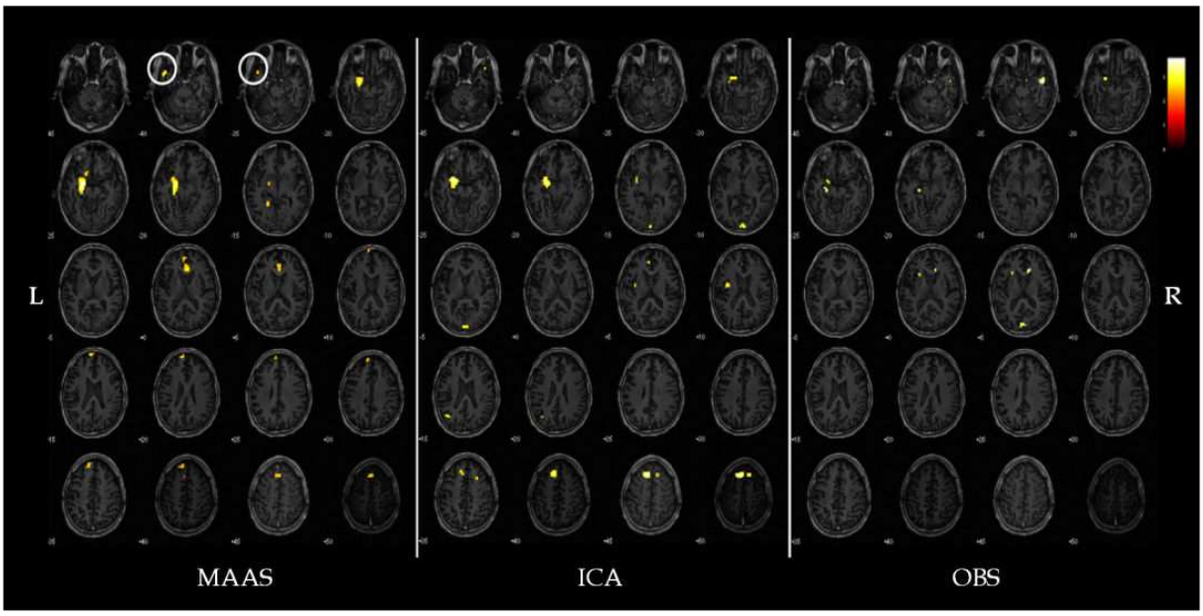

Figure 6. Activation regions from fMRI analysis after removing the BCG artefacts from the measured EEG signal using the MAAS, ICA, and OBS algorithms. The activation regions corresponding to the PEZ is marked with circles.

After post-processing, neurologists detected IEDs from the BCG-artefact removed EEG signals. To localize the IED regions in the brain, fMRI analysis was performed using SPM8 with the detected IED timing information. Then, the activated regions from the fMRI were compared to the presumed epileptogenic zone (PEZ), which was also determined by analyzing the EEG signals, PET images and anatomical MR images.

Since the activated regions from the fMRI are analyzed using the detected IEDs, the performance of the BCG artefact removal algorithms can be indirectly evaluated by comparing the fMRI activation regions. In this experiment, the IED regions in the subjects' brain were localized using the regions revealed by the fMRI analysis (Fig.6). IED regions of subject A is shown in Fig. 6. The localized activation regions of three subjects are shown in Table 1. While the detected fMRI activation regions from all three methods produced the same results for subjects B and C, coincident with PEZ, data of subject A produced different results when the

MAAS algorithm was applied. As shown in Fig.6, the left temporal pole of subject A could be only detected when the BCG artefact of the EEG signal was removed by the MAAS algorithm. When the fMRI activation results were compared to the PEZ of subject A, the activation region was coincident with the PEZ only when the MAAS algorithm was applied.

sub	PEZ	activated regions from fMRI		
		MAAS	**ICA**	**OBS**
A	l. ant -mid temporal area	l. limbic lobe, parahipocamppal gyrus	l. frontal lobe, superior frontal gyrus	r. temporal lobe, superior temporal lobe
		l. temporal pole	l. limbic lobe, parahipocamppal gyrus	r. limbic lobe, anterior cingulate
		r. limbic lobe, anterior cingulate	r. frontal lobe, superior frontal gyrus	l. limbic lobe, parahipocamppal gyrus
		l. frontal lobe, inferior frontal gyrus	r. occipital lobe, lingual gyrus	l. occipital lobe, cuneus
		left frontal lobe, superior frontal gyrus		
B	r. mid - temporal area	r. frontal lobe, middle frontal gyrus r. frontal lobe, inferior frontal gyrus r. temporal lobe, middle temporal gyrus		
C	bifrontal area	r. frontal lobe, middle frontal gyrus r. frontal lobe, superior frontal gyrus		

Table 1. Localization of the IEDs based on the fMRI activation regions

As the results demonstrate, the MAAS algorithm outperforms the other algorithms in this study with epilepsy patients. In spite of its complex calculation, the ICA algorithm cannot clearly detect and remove the BCG artefacts because it cannot sufficiently account for the deviations of spatial information of the BCG artefacts (Debener et al., 2007). On the other hand, the timing information of every R peak is used to estimate the onset and duration of the corresponding BCG artefact more accurately in the MAAS algorithm. Since variation of a subject's heartbeat may alter the delay time of the BCG artifact in the EEG signal from the R peak in the ECG signal (Shin, et al., 2009; Assecondi et al., 2009), the BCG artefacts cannot be fully removed if a fixed delay is used for the BCG artefact detection, such as in the OBS method. Another advantage of the MAAS algorithm is that it uses individual window sizes when subtracting the BCG artefact template from the EEG signal. Since the OBS method uses the mean R-R interval as the window size for the BCG template, the correction result can be distorted if the current R-R interval is shorter than the mean R-R interval. In other words, some

http://dx.doi.org/10.5772/31194

regions may be subtracted twice as it experiences an overlapping of successive subtraction windows.

The simultaneous fMRI-EEG experiment for epilepsy patient enables various types of analysis for research and diagnosis. In clinical fields, simultaneous fMRI-EEG measurement can be used for localization of the epileptic source in presurgical evaluation (Zijlmans et al., 2007) or in epilepsy surgery (Thornton et al., 2010). For research purposes, it can be used to study absence seizures (Moeller et al., 2009), temporal lobe interictal spikes heterotopias (Kobayashi et al, 2006a), startle epilepsy (Fernández et al., 2011), and gray matter heterotopias (Kobayashi et al, 2006b). However, the BOLD changes are related to the detected IEDs with only about 67% accuracy (Al et al. 2003; Krakow, et al., 2001; Salek-Haddadi et al., 2006), possibly due to significant difference in hemodynamic response function (HRF) of epilepsy and the standard HRF model (Bénar et al., 2001). To account for this problem, various HRFs have been developed for epilepsy (Bagshaw et al., 2004; Grouiller et al., 2010).

5. Conclusion

In this chapter, principles and applications for simultaneous fMRI and EEG measurement were discussed. The simultaneous fMRI and EEG measurements can both provide high spatial and temporal resolution, and thus, can generate valuable data for experimental and clinical neuroscientists. However, there are certain problems, such as the IAA and the BCG artefacts, which have to be carefully handled to make a full use of the methodology. If a proper elimination method is employed to reduce possible artefacts in the fMRI and EEG signals, the simultaneous measurement can become a useful tool in various clinical and system neuroscience studies. Thus, a combined analysis of fMRI and EEG will provide a more promising future for elucidating the mechanisms of brain than the separate application of these two tools.

Acknowledgements

This work was partly supported by National Research Foundation of Korea (NRF) grant funded by the Korea government (MEST) (No. 2012-0000125) and by Basic Science Research Program through the NRF grant funded by the Ministry of Science, ICT & Future Planning (NRF-2013R1A1A3009909).

Author details

Yeji Han[1], Sung Suk Oh[1], Joong Koo Kang[2] and HyunWook Park[1]

1 Korea Advanced Institute of Science and Technology, Republic of Korea

2 Asan Medical Center, Republic of Korea

References

[1] Allen, P.J., Polizzi, G., Krakow, K., Fish, D.R., & Lemieux, L. (1998). Identification of EEG Events in the MR Scanner: the Problem of Pulse Artefact and a Method for its Subtraction. *NeuroImage*, Vol.8, No.3, pp.229-239, ISSN 1053-8119

[2] Allen, P.J., Josephs, O., & Turner, R. (2000). A Method for Removing Imaging Artifact from Continous EEG Recorded During Functional MRI. *Neuroimage,* Vol.12, pp.230–9, ISSN 1053-8119

[3] Assecondi, S., Hallez, H., Staelens, S., Bianchi, A.M., Huiskamp, G.M., & Lemahieu, I. (2009). Removal of the Ballistocardiographic Artifact from EEG-fMRI Data: a Canonical Correlation Approach. *Physics in Medicine and Biology*, Vol.54, pp.1673-1689, ISSN 0031-9155

[4] Bagshaw, A.P., Aghakhani, Y., Bénar C.G., Kobayashi, E., Hawco, C., Dubeau, F., Pike, G.B., & Gotman, J. (2004). EEG-fMRI of Focal Epileptic Spikes: Analysis with Mmultiple Haemodynamic Functions and Comparison with Gadolinium-Enhanced MR Angiograms, *Human Brain Mapping*, Vol.22, pp.179–192, ISSN 1065-9471

[5] Bell, A.J. & Sejnowski, T.J. (1995). An Information-Maximization Approach to Blind Separation and Blind Deconvolution. *Neural Computation*, Vol.7, No.6, pp.1129-1159, ISSN 0899-7667

[6] Belouchrani, A., Abed-Meraim, K., Cardoso, J.F., & Moulines, E. (1993). Second-Order Blind Separation of Temporally Correlated Sources. *Proceedings of International Conference on Digital Signal Processing*, Cyprus, pp.346-351.

[7] Bénar, C.G., Gross, D.W., Wang, Y., Petre, V., Pike, B., Dubeau, F., & Gotman, J. (2001). The BOLD Resoponse to Interictal Epileptiform Discharge, *NeuroImage,* Vol. 17, pp.1182-1192, ISSN 1053-8119

[8] Bénar, C., Aghakhani, Y., Wang, Y., Izenberg, A., Al-Asmi, A., Dubeau, F., & Gotman, J. (2003). Quality of EEG in Simultaneous EEG-fMRI for Epilepsy. *Clinical Neurophysiology*, Vol.114, No.3, pp.569-580, ISSN 1388-2457

[9] Bonmassar, G., Purdon, P.L., Jaaskelainen, I.P., Chiappa, K., Solo, V., Brown, E.N., & Belliveau, J.W. (2002). Motion and Ballistocardiogram Artifact Removal for Interleaved Recording of EEG and EPs during MRI. *NeuroImage,* Vol.16, No.4, pp. 1127-1141, ISSN 1053-8119

[10] Cardoso, J.F. & Souloumiac, A. (1993). Blind Beamforming for Non-Gaussian Signals. *IEE Proceedings F Radar and Signal Processing*, Vol.140, No.6, pp.362-370, ISSN 0956-375X

[11] Debener, S., Strobel, A., Sorger, B., Peters, J., Kranczioch, C., Engel, A.K., & Goebel, R. (2007). Improved Quality of Auditory Event-Related Potentials Recorded Simulta-

neously with 3T fMRI: Removal of the Ballistocardiogram Artefact. *NeuroImage,* Vol. 34, pp.587–597, ISSN 1053-8119

[12] Debener, S., Mullinger, K.J., Niazy, R.K., & Bowtell, R.W. (2008). Properties of the Ballistocardiogram Artefact as Revealed by EEG Recordings at 1.5, 3 and 7 Tesla Static Magnetic Field Strength. *International Journal of Psychophysiology*, Vol.67, No.3, pp. 189–199, ISSN 0167-8760

[13] Debener, S., Kranczioch, C., & Gutberlet, I. (2010). EEG Quality: Origin and Reduction of the EEG Cardiac-Related Artefact, In: *EEG-fMRI Physiological Basis, Technique, and Applications*, Christoph Mulert and Louis Lemieux, pp.135-151, ISBN 978-3-540-87918-3, Germany

[14] Deburchgraeve, W., Cherian, P.J., De Vos, M., Swarte, R.M., Blok, J.H., Visser, G.H., Govaert, P., & Van Huffel, S. (2008). Automated Neonatal Seizure Detection Mimicking a Human Observer Reading EEG. *Clinical Neurophysiology*, Vol.119, No.11, pp. 2447–2454, ISSN 1388-2457

[15] Ellingson, M.L., Liebenthal, E., Spanaki, M.V., Prieto, T.E., Binder, J.R., & Ropella, K.M. (2004). Ballistocardiogram Artifact Reduction in the Simultaneous Acquisition of Auditory ERPS and fMRI. *NeuroImage,* Vol.22, No.4, pp.1534-1542 ISSN 1053-8119

[16] Fernández, S., Donaire, A., Maestro, I., Seres, E., Setoain, X., Bargalló, N., Rumià, J., Boget, T., Falcón, C., & Carreño, M. (2011). Functional Neuroimaging in Startle Epilepsy: Involvement of a Mesial Frontoparietal Network. *Epilepsia*, Early View, ISSN 0013-9580

[17] Fisch, B. J. (1999). *Fisch and Spehlmann's EEG Primer: Basic Principles of Digital and Analog EEG* (3rd Edition), Elsevier, ISBN 978-0-444-82148-5, Amsterdam.

[18] Garreffa, G., Bianciardi, M.D., Hagberg, G.E., Macaluso, E., Marciani, M.G., Maraviglia, B., Abbafati, M., Carni, M., Bruni, I., & Bianchi, L. (2004). Simultaneous EEG–fMRI Acquisition: How Far Is It from Being a Standardized Technique?. *Magnetic Resonance Imaging*, Vol.22, No.10, pp.1445-1455, ISSN 0730-725X

[19] Goldman, R.I., Stern, J.M., Engel Jr., J., & Cohen, M.S. (2000). Acquiring Simultaneous EEG and Functional MRI. *Clinical Neurophysiology*, Vol.111, No.11, pp.1974-1980, ISSN 1388-2457

[20] Grouiller, F., Vercueil, L., Krainik, A., Segebarth, C., Kahane, P., & David, O. (2010). Characterization of the Hemodynamic Modes Associated with Interictal Epileptic Activity Using a Deformable Model-Based Analysis of Combined EEG and Functional MRI Recordings. *Human Brain Mapping*, Vol.31, pp.1157–1173 ISSN 1065-9471

[21] Hoffmann, A., Jaejer, L., Werhahn, K.F., Jaschke, M., Noachtar, S., & Reiser, M. (2000). Electroencephalography During Functional Echo-Planar Imaging: Detection of Epileptic Spikes Using Post-processing Methods. *Magnetic Resonance in Medicine,* Vol.44, pp.791-798, ISSN 0740-3194

[22] Huang-Hellinger, F., Breiter, H. C., McCormack, G., Cohen, M. S., Kwong, K. K., Sutton, J. P., Savoy, R. L., Weisskoff, R. M., Davis, T. L., Baker, J. R., Belliveau, J. W., & Rosen, B. R. (1995). Simultaneous Functional Magnetic Resonance Imaging and Electrophysiological Recording. *Human Brain Mapping*, Vol.3, pp.13–23, ISSN 1065-9471

[23] Hyvärinen, A. & Oja, E. (2000). Independent Component Analysis: Algorithms and Applications. *Neural Networks*, Vol.13, No.4-5, pp.411-430 ISSN 0893-6080

[24] In, M.H., Lee, S.Y., Park, T.S., Kim, T.S., Cho, M.H., & Ahn, Y.B. (2006). Ballistocardiogram Artifact Removal from EEG Signals Using Adaptive Filtering of EOG Signals. *Physiological Measurement*, Vol.27, pp.1227-1240

[25] Ives, J.R., Warach, S., Schmitt, F., Edelman, R.R., & Schomer, D.L. (1993). Monitoring the Patient's EEG During Echo Planar MRI. *Electroencephalography and Clinical Neurophysiology*, Vol.87, No.6, pp.417–20, ISSN 1388-2457

[26] Kim, K.H., Yoon, H.W., & Park, H.W. (2004). Improved Ballistocardiac Artifact Removal from the Electroencephalogram Recorded in fMRI. *Journal of Neuroscience Methods*, Vol.135, No.1-2, pp.193-203

[27] Kobayashi, E., Bagshaw, A.P., Benar, C.G., Aghakhani, Y., Andermann, F., Dubeau, F., & Gotman, J. (2006a). Temporal and Extratemporal BOLD Responses to Temporal Lobe Interictal Spikes. *Epilepsia*, Vol.47, pp.343–354, ISSN 0013-9580

[28] Kobayashi, E., Bagshaw, A.P., Grova, C., Gotman, J., & Dubeau, F. (2006b). Grey Matter Heterotopia: What EEG-fMRI Can Tell Us About Epileptogenicity of Neuronal Migration Disorders, *Brain*, Vol.129, pp.366–374.

[29] Koskinen, M. & Varitiainen, N. (2009). Removal of Imaging Artifacts in EEG during Simultaneous EEG/fMRI Recording: Reconstruction of a High-Precision Artefact Template. *Neuroimage*, Vol.46, pp.160-167, ISSN 1053-8119

[30] Krakow, K., Lemieux, L., Messina, D., Scott, C.A., Symms, M.R., Duncan, J.S., & Fish, D.R. (2001). Spatio-Temporal Imaging of Focal Interictal Epileptiform Activity Using EEG-Triggered Functional MRI. Epileptic Disorders, Vol.3, pp.67–74, ISSN 1950-6945

[31] Lemieux, L., Allen, P.J., Franconi, F., Symms, M.R., & Fish, D.R. (1997). Recording of EEG During fMRI Experiments: Patient Safety. *Magnetic Resonance in Medicine*, Vol. 38, No.6, pp.943–52, ISSN 0740-3194

[32] Mantini, D., Perrucci, M.G., Cugini, S., Ferretti, A., Romani, G.L., & Del Gratta, C. (2007). Complete Artifact Removal for EEG Recorded During Continuous fMRI Using Independent Component Analysis. *NeuroImage*, Vol.34, pp.598–607, ISSN 1053-8119

[33] Masterton, R.A., Abbott, D.F., Fleming, S.W., & Jackson G.D. (2007). Measurement and Reduction of Motion and Ballistocardiogram Artefacts from Simultaneous EEG and fMRI Recordings. *Neuroimage*, Vol.37, pp.202-211, ISSN 1053-8119

[34] Moeller, F., LeVan, P., Muhle, H., Stephani, U., Dubeau, F., Siniatchkin, M., & Gotman, J. (2010). Absence Seizures: Individual Patterns Revealed by EEG-fMRI, *Epilepsia,* Vol.51, No.10, pp.2000-10, ISSN 0013-9580

[35] Mullinger, K., Debener, S., Coxon, R., Bowtell, R. (2008). Effects of Simultaneous EEG Recording on MRI Data Quality at 1.5, 3 and 7 tesla. *International Jounal of Psychophysiology*, Vol.67, No.3, pp.178-188, ISSN 0167-8760

[36] Niazy, R.K., Beckmann, C.F., Iannetti, G.D., Brady, J.M., & Smith, S.M. (2005). Removal of FMRI Environment Artifacts From EEG Data Using Optimal Basis Sets. *NeuroImage*, Vol.28, pp.720–737, ISSN 1053-8119

[37] Oh, S-S, Han, Y., Lee, J., Yun, S.D., Kang, J.K., Lee, E.M., Yoon, H.W., Chung, J.Y., Park, H.W. (2014). A Pulse Artifact Removal Method Considering Artifact Variations in the Simultaneous Recording of EEG and fMRI. Neuroscience Research, Vol.81-82, pp.42-50, ISSN 0168-0102

[38] Reilly, E.L. (2005). EEG Recording and Operation of the Apparatus. In: *Electroencephalography: Basic Principles, Clinical Applications and Related Fields*. Ernst Niedermeyer and Frenando Lopes da Silva, pp.139-160, Lippincott Williams & Wilkins, ISBN 0-7817-5126-8, Philadelphia.

[39] Ritter, P., Becter, R., Freyer, F., & Villringer, A. (2010). EEG Quality: The Image Acquisition Artefact, In: *EEG-fMRI Physiological Basis, Technique, and Applications*, Christoph Mulert and Louis Lemieux, pp.153-171, ISBN 978-3-540-87918-3, Germany

[40] Rosenkranz, K. & Lemieux, L. (2010). Present and Future of Simultaneous EEG-fMRI. *Magnetic Resonance Materials in Physics, Biology and Medicine*, Vol.23. pp.309-316, ISSN 0968-5243

[41] Salek-Haddadi, A., Diehl, B., Hamandi, K., Merschhemke, M., Liston, A., Friston, K., Duncan, J.S., Fish, D.R., & Lemieux, L. (2006). Hemodynamic Correlates of Epileptiform Discharges: An EEG-fMRI Study of 63 Patients with Local Epilepsy. *Brain Research*, Vol.1088, No.1, pp.148-166, ISSN 0006-8993

[42] Sharieff, G.Q. & Rao, S.O. (2006). The Pediatric ECG, *Emergency Medicine Clinics of North America*, Vol.24, pp.195-208, ISSN 0733-8627

[43] Shin, J.H., Lee, K.M., & Park, K.S. (2009). Non-Constrained Monitoring of Systolic Blood Pressure on a Weighing Scale, *Phyiological Mesurement*, Vol.30, pp.679-693, ISSN 0967-3334

[44] Sijbers, J., Michiels, I., Verhoye, M., Van Audekerke, J., Van der Linden, A., & Van Dyck, D. (1999). Restoration of MR-Induced Artifacts in Simultaneously Recorded MR/EEG Data. *Magnetic Resonance Imaging*, Vol.17, No.9, pp.1383–1391, ISSN 0730-725X

[45] Sijbers, J., Van Audekerke, J., Verhoye, M., Van der Linden, A., & Van Dyck, D. (2000). Reduction of ECG and Gradient Related Artifacts in Simultaneously Recorded

Human EEG/fMRI Data. *Magnetic Resonance Imaging*, Vol.18, No.7, pp.881-886, ISSN 0730-725X

[46] Srivastava, G., Crottaz-Herbette, S., Lau, K.M., Glover, G.H., & Menon, V. (2005). ICA-Based Procedures for Removing Ballistocardiogram Artifacts from EEG Data Acquired in the MRI Scanner. *NeuroImage*, Vol.24, No.1, pp.50-60, ISSN 1053-8119

[47] Tenforde, T.S., Gaffey, C.T., Moyer, B.R., & Budinger, T.F. (1983). Cardiovascular Alterations in Macaca Monkeys Exposed to Stationary Magnetic Fields: Experimental Observations and Theoretical Analysis. *Bioelectromagnetics*, Vol.4, No.1, pp.1-9, ISSN 1521-186X

[48] Thornton, R., Laufs, H., Rodionov, R., Cannadathu, S., Carmichael, D.W., Vulliemoz, S., Salek-Haddadi, A., McEvoy, A.W., Smith, S.M., Lhatoo, S., Elwes, R.D., Guye, M., Walker, M.C., Lemieux, L., & Duncan, J.S. (2010). EEG Correlated Functional MRI and Postoperative Outcome in Focal Epilepsy. *Journal of Neurology, Neurosurgery, and Psychiatry*, Vol.81, pp.922–927, ISSN 0022-3050

[49] Vanderperren, K., De Vos, M., Ramauter, J., Novitskiy, N., Mennes, M., Assecondi, S., Vanrumste, B., Stiers, P., Van den Bergh, B., Wagemans, J., Lagae, L., Sunaert, S. & Van Huffel, S. (2010). Removal of BCG Artifacts from EEG Recordings Inside the MR Scanner: A Comparison of Methodological and Validation-Related Aspects. *NeuroImage*, Vol.50, No.3, pp.920-934, ISSN 1053-8119

[50] Vincent, J.L., Larson-Prior, L.F., Zempel, J.M., Snyder, A.Z. (2007). Moving GLM Ballistocardiogram Artifact Reduction for EEG Acquired Simultaneously with fMRI. *Clinical Neurophysiology*, Vol.118, No.5, pp.981-998, ISSN 1388-2457

[51] Zijlmans, M., Huiskamp, G., Hersevoort, M., Seppenwoolde, J.H., van Huffelen, A.C., & Leijten, F.S. (2007). EEG-fMRI in the Preoperative Work-Up for Epilepsy Surgery. Brain, Vol.130, pp.2343–2353, ISSN 1460-2156